INVITED PAPER

Physical and Chemical Sensing With Electronic Skin

By Kuniharu Takei, *Member IEEE*, Wei Gao, Chuan Wang, and Ali Javey

ABSTRACT | This paper reviews current progress on flexible and stretchable transistors and sensors for the next-generation multiplex electronics (commonly referred to as "electronics skin" or "e-skin") that is capable of simultaneous detection of multiple information from a variety of surfaces including human skin. Flexible chemical sensors for sweat analysis as well as physical sensors for detecting tactile force, bending, and temperature will be discussed, with emphasis on materials, detection mechanisms, and device demonstration to realize multiplex human-interactive devices. Next, system integration enabling the real-time monitoring of health conditions is also demonstrated as a proof of concept. Finally, perspectives on e-skin for moving toward realizing practical wearable electronics in the market are discussed. This paper targets the translation of the nano- and flexible technologies from academic innovations to industrial practical applications with high-impact breakthroughs.

KEYWORDS | Chemical sensors; electronic skin; flexible electronics; physical sensors

I. INTRODUCTION

Dynamic physiological monitoring is essential to the realization of personalized medicine through continuously collecting large sets of data from people's daily activities and capturing meaningful health status changes in time for preventive intervention. There is an urgent need for wearable devices that can perform personalized physical and molecular monitoring to provide an in-depth understanding of the physiological status of an individual. In addition, the motion artifacts and mechanical mismatches between conventional rigid electronic materials and soft skin often lead to substantial errors in collected data. Thus, it will be of great importance to develop wearable and flexible electronic systems that could be conformally in contact with the skin and integrate the sensing capabilities for accurate dynamic health assessment.

Recent years, tremendous progress has been made in flexible electronic skin (commonly referred to as "e-skin") that has unique advantages including high transparency, lightweight, low cost, high flexibility, and stretchability [1]–[6]. The innovations in materials, fabrication processes, and sensing strategies have played a significant role in the development of the next-generation e-skin-based devices toward physical and chemical sensing [1]–[10]. Many applications that utilize the e-skin concept have been proposed such as healthcare [7], [8], [11], [12], robotics [13]–[15], and Internet of Things (IoT) [16], [17]. The e-skin concepts include not only multimodality physical and chemical sensing but also the interaction with human and other objects based on the real-time analysis of sensing data [14]. Another important consideration for wearable or biomedical application is comfort and flexibility due to direct contact to the human body. To address many challenges for the next class of electronics, macroscale and multifunctional flexible and/or stretchable devices need to be developed by applying a variety of materials, structures, fabrication technologies, and concepts.

In this paper, we will review the current progress on e-skin starting with flexible and stretchable transistors and sensors for the next-generation wearable and flexible electronics that are capable of simultaneous detection of multiple information from a variety of surfaces including

Manuscript received December 19, 2018; revised March 1, 2019; accepted March 20, 2019. *(Corresponding author: Kuniharu Takei.)*

K. Takei is with the Department of Physics and Electronics, Osaka Prefecture University, Osaka 599-8531, Japan (e-mail: takei@pe.osakafu-u.ac.jp).

W. Gao is with the Division of Engineering and Applied Science, California Institute of Technology, Pasadena, CA 91125 USA (e-mail: weigao@caltech.edu).

C. Wang is with the Department of Electrical and Systems Engineering, Washington University in St. Louis, St. Louis, MO 63130 USA (e-mail: chuanwang@wustl.edu).

A. Javey is with the Department of Electrical Engineering and Computer Sciences, University of California at Berkeley, Berkeley, CA 94720 USA (e-mail: ajavey@berkeley.edu).

Digital Object Identifier 10.1109/JPROC.2019.2907317

human skin. Flexible chemical sensors for sweat analysis as well as physical sensors for detecting tactile force, bending, and temperature will be discussed, with emphasis on materials, detection mechanism, and device demonstration to realize multiplex human-interactive devices. Perspectives on e-skin for moving toward realizing practical wearable electronics in the market will also be discussed.

II. PHYSICAL TACTILE PRESSURE SENSING E-SKIN

A. Flexible E-Skin

Flexible e-skins consisted of the arrays of tactile pressure sensors and/or temperature sensors have been widely studied by using organic and inorganic materials [1], [2], [18]–[23]. Two types of the device backplanes, active matrix and passive matrix, are mainly used depending on the applications and requirements. Active-matrix backplane integrated with switching transistors to select a pixel has better resolution compared to the passive one. This is because the crosstalk from the other sensors can be suppressed drastically. For the passive matrix, the advantage is that the device structure is simple. To achieve macroscale and low-cost processes for the active matrix system, organic-based transistors are often used [1], [4], [24]. Organic semiconducting materials can be formed by solution-based processes resulting in good scalability. However, the mobility of organic transistors still needs to be improved to realize a low-power operation. In contrast, macroscale printing and transferring processes of inorganic nanomaterials have been proposed to realize high mobility and stable transistors [2], [25], [26]. Due to the nanosize of the materials, the inorganic-based transistors can be mechanically flexible for the purpose of e-skin applications [27]. In fact, nanowires (NWs) [2], nanotubes [25], and 2-D material systems [26] have been used to develop the active-matrix backplane e-skin. In this paper, NW-based e-skin is discussed in detail.

Flexible e-skin capable of tactile pressure sensing has been demonstrated based on active-matrix backplane using Ge/Si core/shell NW arrays on a polyimide film [2]. The NW arrays can be used to form p-type semiconductor thin-film transistors (TFTs) that act as switches in an active matrix for pixel selection. Pressure detection is realized using a commercially available pressure-sensitive rubber (PSR). An 18 $\times$ 19 array of pressure sensors with active matrix transistors was fabricated by optimizing device process and materials [Fig. 1(a)]. Ge/Si NW arrays were printed between source (S) and drain (D) electrodes as the transistor channel materials with a density of $\sim$5 NWs/μm, as shown in Fig. 1(b). Due to strong Van der Waals interaction between NWs and SiO_x layer formed on the polyimide film, the NW array is stably formed during the device fabrication process. Each pixel comprises a transistor and PSR [Fig. 1(c)]. Field-effect mobility of NW-based flexible transistor is $\sim$20 cm^2/Vs. It should be noted that the

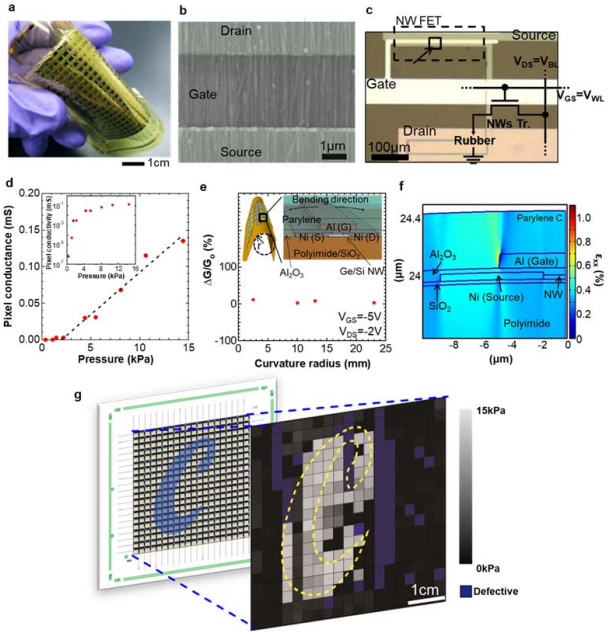

Fig. 1. ***NW-based active-matrix backplane e-skin. (a) Photograph of 18 $\times$ 19 pixel array e-skin. (b) SEM image of Ge/Si core/shell NW array transistor. (c) Optical microscope image of a pixel. (d) Pixel conductance as a function of applied tactile pressure. (e) on-state conductance change ratio under mechanical bending of the transistors up to 2.5-mm radius. (f) FEM simulation of strain distribution under 2.5-mm bending radius. (g) Pressure distribution measured from the NW-based active-matrix backplane e-skin. Reproduced with permission from [2]. Copyright 2010 Nature Publishing Group.***

ON-state conductance of the transistor should be much higher than that of the PSR in order to monitor precise tactile pressure change. To achieve this, transistors with a relatively wide channel ($\sim$250 μm) were designed, resulting in a transistor with ON-state conductance of $\sim$0.34 mS that is higher than the one of the PSR.

Tactile pressure detection was achieved by measuring the conductance change of the PSR through the transistor. The PSR consists of a conductive nanocarbon material in an elastomer matrix. The matrix conductance determined by the tunneling current between the nanocarbon fillers varies as a function of tactile pressure applied on the PSR. The pixel conductance increased drastically after the pressure exceeded 3 kPa, suggesting that the distance between nanocarbons in the rubber was small enough to cause tunnel current. At >3 kPa, the conductance increased linearly with increasing pressure as shown in Fig. 1(d). The sensor sensitivity extracted from the linear fitting above 3 kPa is $\sim$11.5 μS/kPa. Because this e-skin can detect relatively small tactile pressure of a few kilopascals that is similar to the pressure exerted by fingers when typing a keyboard, it can potentially be used to imitate human skin for robotics applications. The response time of the e-skin is $\sim$0.1 s, which is almost the same as the speed of the pressure input from the experimental setup

used in this paper. However, this time could be much faster because the response time is limited by the relaxation time of the elastomer in the PSR.

For many e-skin applications, mechanical flexibility and robustness of the devices are also important factors besides the sensing sensitivity. Conductance change of the NW flexible transistor was characterized under mechanical bending as a function of curvature radius down to 2.5 mm [Fig. 1(e)]. The bending direction was along the channel length direction between the S/D electrodes. The maximum conductance change ($\Delta G/G_0$, where $\Delta G = G_0 - G$, G and G_0 are the conductance at bending and flat states, respectively) was ~6% at a radius of 2.5 mm. This small change was most likely caused by a strain in the NW channel of ~0.35% extracted from a finite-element method (FEM) simulation [Fig. 1(f)]. Because the applied pressure induced much larger conductance change in the PSR, this strain effect on the transistor conductance became negligible. The robustness of the device was also confirmed without having delamination or breakage after at least 2000 bending cycles.

As a proof-of-concept demonstration of using the NW transistor-based active matrix e-skin for spatial mapping of tactile pressure distribution, an 18 × 19 array with a size of 7 × 7 cm^2 on polyimide film was used to measure the pressure from a "C"-shaped object with applied normal pressure of around 15 kPa. As expected, the pressure distribution measured by the active matrix e-skin resembled the object placed on top. In addition, due to the use of active-matrix backplane design, crosstalk effects from adjacent pixels were minimized, resulting in high spatial resolution for tactile pressure monitoring.

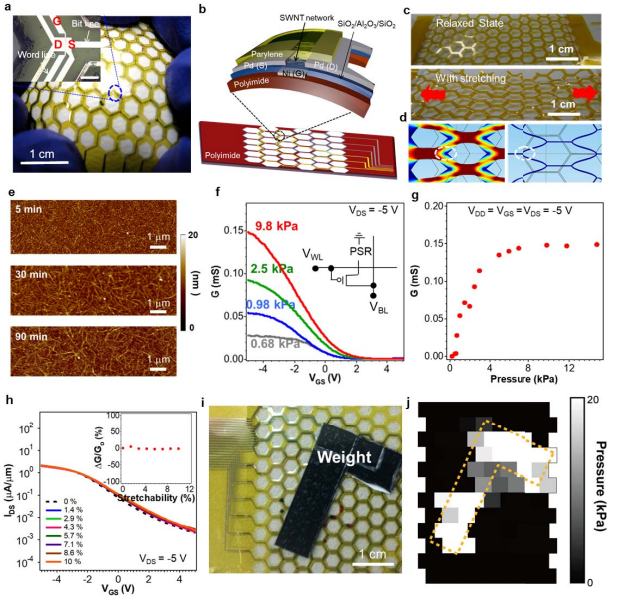

Fig. 2. ***Stretchable e-skin with CNT-based active matrix circuits. (a) Photograph of the stretchable e-skin covered over a baseball. (b) Schematic of the honeycomb polyimide structure and CNT transistor. (c) Photograph of the honeycomb structure polyimide at relaxed state (top) and stretching state (bottom). (d) FEM simulation of stress under 2-mm stretch with wider (left) and shallower (right) honeycomb width. (e) Atomic force microscopy images of CNT networks at different deposition times. (f) Pixel conductance at different applied tactile pressure as a function of VGS. (g) Conductance change at applied pressure. (h) CNT transistor characteristics under stretching condition up to 10%. (i) Photograph and (j) output signal of pressure distribution monitoring. White dashed circles: almost zero-stress region under stretching deformation. Reproduced with permission from [25]. Copyright 2011 American Chemical Society.***

B. Stretchable E-Skin

Mechanical stretchability is another important function to cover 3-D objects and also movable objects like human bodies. Two strategies can be used to realize mechanical stretchability in the e-skin. The first one is to make all materials used in the sensors and transistors intrinsically stretchable. To achieve stable and reliable sensing results, the material formation is challenging but good progress has been made, as will be reviewed in later sections of this paper. The second approach is to use structural design to achieve stretchability for only the substrate. In this case, active materials need to be strain free under mechanical deformation based on the strain engineering. This section focuses on the second approach due to simple and reliable approaches in this present technology.

For this approach, a serpentine metal structure is used to be stretchable without causing delamination and cracks in the devices [3], [15]. Another approach is to arrange the film structures such as kirigami and honeycomb shape of unstretched films. In particular, the polyimide substrate is designed to have a honeycomb shape formed by a laser cutter, and the transistors using organic and inorganic materials are formed on the place where it is almost strain free under stretching conditions [1], [25]. As an example, carbon nanotube (CNT)-based stretchable e-skin with the honeycomb shape of a polyimide film is discussed. CNT-based transistors were formed on the vertices of the honeycomb to reduce the strain under stretching condition, as displayed in Fig. 2(a) and (b). Using this structure, the polyimide films with transistors can be covered conformably over a baseball without having cracking and delamination [Fig. 2(a)]. To understand strain distribution under stretching, two types of honeycomb structures were fabricated and simulated using FEM simulations for stress observations. Fig. 2(c) shows that the film is stretchable, which is enabled by the structure change of the honeycomb structure. Smaller width of the honeycomb structure in the polyimide film leads to more flexible and stretchable film. Strain distribution of both samples under 2-mm stretch is shown in Fig. 2(d). First, the polyimide with honeycombs of smaller width has much less stress compared to the one with a larger width. Second, the vertices of the honeycomb pattern highlighted with a white circle in Fig. 2(d) exhibit almost zero stress for honeycomb structure with both widths. Utilizing this strain engineering, flexible

TFTs can be strategically fabricated at the vertices on the honeycomb polyimide substrate to prevent them from being affected by large tensile stress when the sample is stretched.

To achieve uniform and high-performance flexible transistors, semiconductor-enriched CNT network film was developed. The density of the CNT network can be controlled by the deposition time as shown in Fig. 2(e) [25]. This density difference affects the ON-current and transconductance (corresponding to the field-effect mobility), as well as I_{ON}/I_{OFF} ratio of the devices. For higher density CNTs, ON-current is increased while I_{ON}/I_{OFF} ratio is decreased due to high OFF-current caused by the bundling of CNTs. The average mobility, log (I_{ON}/I_{OFF}), and threshold voltage change from 16 to 26 cm^2/Vs, 6 to 2.4, and -4.6 to -5.0 V, respectively, when the CNT deposition time is increased from 5 to 90 min. By integrating a PSR with a CNT transistor in series, output conductance changes as a function of applied pressure due to the resistance change of the PSR [Fig. 2(f) and (g)]. Briefly, the conductance increases almost linearly with increasing pressure from 0 to 6 kPa and then saturates at above 6 kPa, which is limited by the dynamic range of pressure detection of the PSR.

After confirming the fundamental pixel operation, the stretchability for the integrated CNT transistor active-matrix backplane was investigated. Under the tensile strain of up to 10%, the transistor characteristics remained almost unchanged, as shown in Fig. 2(h). As described earlier, the stable and robust operation of the transistors was realized by placing the transistor at almost stress-free regions under stretch. However, for this honeycomb structure, the strain of above 10% causes damage to the polyimide film. If more stretchability is required, the honeycomb width should be smaller.

Finally, the stretchable e-skin was used to monitor pressure distribution by applying a pressure of up to 20 kPa, as shown in Fig. 2(i). The stretchable e-skin is comprised of 12 $\times$ 8 pixels and all pixels worked without any malfunction. To obtain the pressure mapping, each pixel was addressed by turning the pixel transistor on, and the result is shown in Fig. 2(j). Due to the large size of pixel limited by the honeycomb structure of the polyimide film, the resolution is not high enough to accurately reflect the shape object. However, pressure distribution was clearly obtained. To improve the resolution, transistor size and honeycomb structure need to be shrunk down.

C. Human-Interactive Responsive E-Skin

In addition to combining a variety of sensing modalities, it is also possible to integrate human-interactive functionalities such as a display or haptic feedback to the e-skin to expand its potential wearable applications. For example, light emission [14] or color changing [28] is effective ways to instantaneously display information about the sensor response to the users. Fig. 3 shows an example of a user-interactive e-skin, in which the pressure

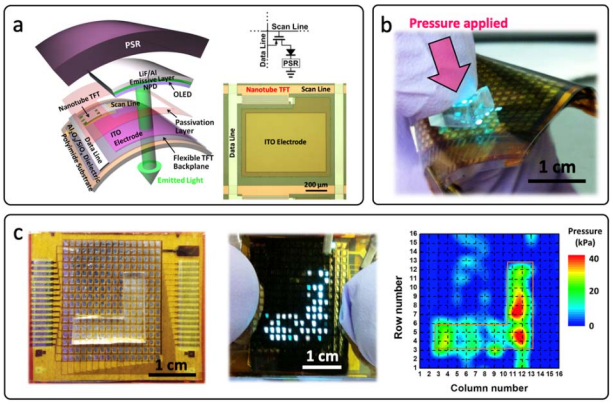

Fig. 3. *User-interactive e-skin. (a) Schematic and optical micrograph showing one pixel of the user-interactive e-skin, comprising a TFT, a pressure sensor, and an OLED. (b) Photograph illustrating the operation of the user-interactive e-skin—the OLED in the pixels is turned on locally when pressure is applied. (c) Mapping of applied pressure using the interactive e-skin with both optical and electrical output. (d) Hydration status analysis using the wearable sweat sensor. The data show high spatial resolution and good agreement between the two sets of outputs. Reproduced with permission from [14]. Copyright 2013 Nature Publishing Group.*

sensors are monolithically integrated with organic light-emitted diodes (OLEDs) in an active-matrix backplane individually addressed by CNT TFTs [14]. As shown in the schematic in Fig. 3(a), each pixel comprises a pressure sensor (PSR) that is connected in series with an OLED. In such a configuration, the externally applied pressure changes the resistance of the PSR and thus the current flowing through the OLED, allowing the applied pressure to be visualized as the emitted light from the OLED. The light intensity qualitatively represents the magnitude of the applied pressure. Fig. 3(b) shows another example where only pixels with pressure applied are turned on. Such human-interactive e-skin enables both electrical readout (by measuring the current in each pixel) and visual feedback of the applied pressure with a high spatial resolution [Fig. 3(c)]. While this example uses a pressure sensor and OLED as a proof-of-concept demonstration, one can easily replace or add other types of sensors such as temperature sensor, photodetector, or sweat sensor to enable more complex functionalities that may find a wide range of applications in wearable health-monitoring devices.

III. E-SKIN FABRICATED BY PRINTING PROCESS

Among the various potential applications of e-skin, many of them have less demanding requirements on device performance and speed compared to modern integrated circuits. The main consideration is instead focused on large-area manufacturability and cost. For example, considering an e-skin is designed to be used as a wearable patch for biomedical applications, if the cost is sufficiently low, it will be feasible to use it as a

disposable device, which is ideal. Conventional processes adapted from the semiconductor industry usually involve photolithographic patterning and vacuum-based deposition and etching processes that are costly. Alternatively, a recent work has demonstrated that printing—a widely used additive manufacturing method—could also be adopted for large-scale and low-cost fabrication of electronic devices and sensors [29], [30]. In addition, printing also enables fabrication on many unconventional substrates including plastics, elastomers, papers, and textiles, which could enable numerous applications ranging from smart packaging to electronic wallpaper and ubiquitous wearable electronics [31]. In this section, we will review progress made on printed TFTs used as switching devices in the active-matrix backplane of the e-skin. We will also cover a variety of printed sensors in the next section.

A. Printed CNT-Based Flexible Transistors

Printing requires various types of materials used in a transistor—metal, insulation, and most importantly semiconductor—to be in solution form and formulated as electronic inks with appropriate concentration, viscosity, vapor pressure, and wetting on the target substrates. A variety of materials have been studied in the printed electronics community. For metal ink, metallic nanoparticles (NPs) (e.g., silver), 1-D metallic NWs or CNTs [32]–[35], 2-D graphene [36], conductive polymer [37], [38], or nanomaterial/polymer composites [39], [40] can be used. Depending on the material, the sheet resistance of the printed film typically ranges from $\sim$10 Ω/sq for metal-based nanomaterials to above 100 Ω/sq for carbon-based materials and conductive polymers. The most widely studied dielectric inks are ion gels [41] and polymer–inorganic NP hybrid dielectrics [42]. Due to the formation of electrical double layers, ion gel offers very large gate capacitance, which is, in principle, independent of the film thickness. Hybrid dielectrics consisting of polymers and inorganic NPs also offer dielectric constants that are significantly better than pure polymer and are also excellent choices for printed transistors. Finally, for the channel semiconductor, organic semiconductors have been widely studied in printed electronics for a long time [43], [44]. More recently, inorganic 1-D [45], [46] or 2-D nanomaterials [47] and metal oxides [48] have also been widely explored for printed electronics, many of which have significantly outperformed organic semiconductor in terms of overall device performance and long-term stability. In particular, solution-processed semiconducting CNTs have shown great promise for high-performance printed TFTs and circuits on flexible substrates. Regarding printing methods, there are also several options available, with inkjet printing [49], [50], gravure printing [51]–[54], aerosol jet printing [41], [55], and screen printing [56] being the most commonly used. Gravure and screen printing are particularly suitable for large-area fabrication, while inkjet and aerosol jet printing are maskless and more flexible for changing the layout design, which is important in a research and development setting. On the other hand, for inkjet and aerosol jet printing, the patterns need to be printed line by line so that the process can be relatively slow. Gravure and screen printing are much faster but they instead require multiple sets of masks that may be costly and also make modifying the design more difficult. Finally, inkjet, aerosol jet, and gravure printing are all additive manufacturing processes, while the screen printing is subtractive meaning that a lot of materials could potentially be wasted. While all the printing methods mentioned above have been used to fabricate printed CNTs TFTs, it is important to consider the pros and cons of each method above and choose the most suitable printing method for a particular application.

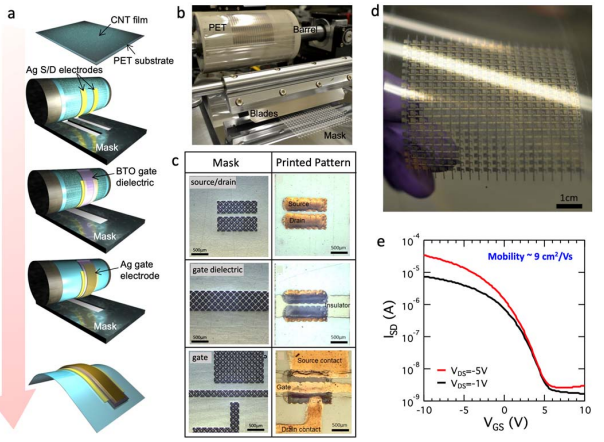

Fig. 4. *Gravure-printed CNT TFT on the plastic substrate. (a) Schematic illustrating the printing process. (b) Photograph of the inverse gravure printer. (c) Mask design and the printed pattern after each printing step. (d) Photograph of a fully printed 20 $\times$ 20 TFT array. (e) Transfer characteristics of a printed TFT. Reproduced with permission from [54]. Copyright 2013 American Chemical Society.*

Fig. 4 shows an example of high-performance flexible CNT TFTs made by gravure printing [54]. The detailed fabrication process is illustrated in Fig. 4(a)–(c), in which the source/drain electrodes, gate dielectric layer, and gate electrode are sequentially printed onto flexible polyethylene terephthalate (PET) substrates in a roll-to-roll or roll-to-plate manner. For such gravure printing processes, the viscosity and surface tension of the inks and surface chemistry of the substrates are critical and need to be optimized to achieve uniform and reproducible device performance. Silver NP ink is widely used as a printable conductor for making the electrodes. The printed gate dielectric layer plays a more crucial role as it directly affects device performance. Because conventional polymers have a low dielectric constant and it is also very difficult to achieve an ultrathin pinhole-free printed dielectric layer with good uniformity and clean interface, the transistors inevitably require a large voltage to operate. In order to address this issue, hybrid dielectrics consisting of polymers and inorganic NPs such as $BaTiO_3$/polymethyl

methacrylate (PMMA) hybrid dielectric can be used [42]. The high dielectric constant of $BaTiO_3$ NPs greatly enhances the dielectric constant of the composite film and thus gate strength, which can lead to high-performance printed transistors. Fig. 4(d) shows the above gravure-printed TFTs being integrated into a 20 × 20 pixel active-matrix backplane, which can be used to drive displays and e-skin. The printed transistors in the active-matrix backplane exhibit high performance with small operating voltage (<10 V), large ON/OFF ratio (>10^4), and a good field-effect mobility of ~9 cm^2/Vs, as shown in Fig. 4(e). In addition to the printed TFT array, integrated arithmetic logic circuits such as logic gates, half-adder, D-flip-flop, and one-bit radio frequency identification (FRID) tags have all been successfully demonstrated using the gravure printing process [51]–[53].

B. Printed Intrinsically Stretchable Transistors

For potential applications in wearable/implantable health monitoring and diagnostic devices, it is desirable to have stretchable e-skin built on soft elastic substrates instead of plastic substrates in order to achieve conformal body surface coverage and minimize motion artifact [3], [5], [6], [57]. Through the use of intrinsically stretchable elastomeric or composite electronic materials that are solution processable, the printing process can also enable large-area and low-cost fabrication of high-performance stretchable electronic devices on elastic substrates such as polydimethylsiloxane (PDMS) [35], [58], [59]. Compared with the silver NP ink used above for the electrodes, CNT thin film is a perfect choice for stretchable electrodes because of its ultra-high aspect ratio and the formation of highly deformable mesh structures in macroscale assemblies [60]. As shown in Fig. 5(a), dense unsorted CNTs can be printed to form the source/drain/gate electrodes, and monolayer of high-purity semiconducting single-walled CNTs (sSWCNTs) can be printed as the channel semiconductor in the TFT [61]. Similar to the concept of the $BaTiO_3$/PMMA hybrid dielectric used in the printed flexible TFT above, the gate dielectric for the stretchable TFT is a composite consisting of PDMS, the same material as the stretchable substrate, and $BaTiO_3$ that offers a high dielectric constant. The dielectric constant of the composite PDMS/$BaTiO_3$ gate dielectric increases monotonically with the increasing volume ratio of $BaTiO_3$ dispersed in PDMS and it goes up to ~9 at 26%. This is significantly better than the dielectric constant of ~2 in pure PDMS and will help to increase the gate strength and reduce the operating voltage in printed transistors. Fig. 5(b) shows the photographs of a representative sample with printed stretchable TFTs and integrated logic circuits that can be stretched by up to 50%. The transistors are able to deliver excellent performance and mechanical robustness, with minimal change in transfer characteristics in both relaxed and stretched states as shown in Fig. 5(c). Key figures of merit of the transistors including carrier mobility and ON/OFF current ratio can be extracted from

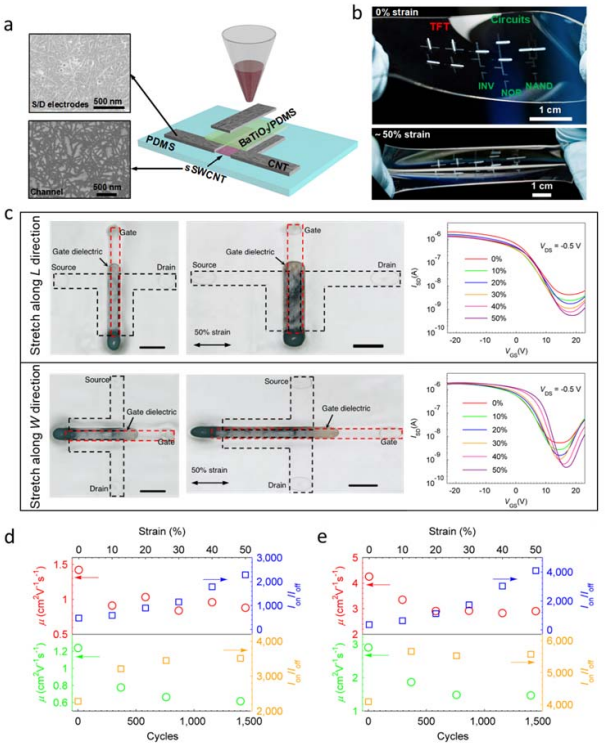

Fig. 5. ***Printed intrinsically stretchable CNT TFT. (a) Schematic illustrating the structure of a printed stretchable TFT. (b) Optical photograph of a representative sample consisting of printed TFTs and logic circuits in a relaxed state (top) and under a tensile strain of ~50% (bottom). (c) Optical micrographs and transfer characteristics of two printed TFTs when stretched along channel length and channel width directions to a tensile strain of up to 50%. Scale bar: 1 mm. (d) and (e) Carrier mobility and on/off current ratio of the printed stretchable TFT as functions of strain and number of stretching cycles when the device is stretched along the channel length (d) and channel width (e) directions, respectively. Reproduced with permission from [61]. Copyright 2016 American Chemical Society.***

the transfer characteristics, and the results are shown in Fig. 5(d) and (e). Such printed stretchable transistors exhibit average mobility of around 4 $cm^2V^{-1}s^{-1}$ and ON/OFF ratio greater than 500 with maximum values of 7 $cm^2V^{-1}s^{-1}$ and 3000, respectively, which is respectable for the all-printing process. Regardless of the stretching direction (along the channel length or channel width directions), the mobility decreases by about 1/3 of its original value when the device is under 50% tensile strain, which can be attributed to the microscopic structural changes in the sSWCNT networks. On the other hand, the ON/OFF ratio increases by almost one order of magnitude at 50% strain due to the significantly suppressed OFF-state current. The devices have been tested for up to 1500 stretching cycles, and the device characteristics remain relatively stable.

C. Printed E-Skin With Active Matrix Circuit for Tactile Sensing

The printed CNT TFTs have also been incorporated in functional electronic systems such as e-skin with

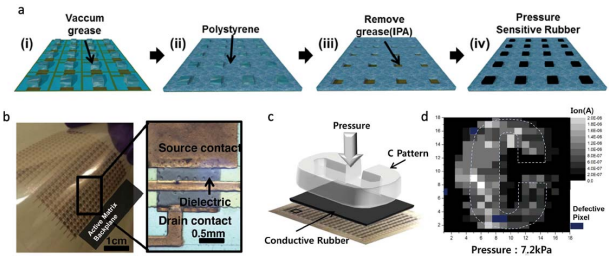

Fig. 6. ***Gravure-printed CNT TFT backplane for applications in e-skin. (a) Schematics illustrating the fabrication process where the PSR is monolithically integrated with the TFT backplane. (b) Printed flexible active-matrix backplane with 20 × 20 pixels. Inset: enlarged view showing a single printed TFT. (c) and (d) E-skin with printed active-matrix backplane for spatial mapping of the applied pressure profile. The measured current in each pixel corresponds to the magnitude of the applied pressure. Reproduced with permission from [62]. Copyright 2015 John Wiley and Sons.***

monolithically integrated pressure sensor arrays. Using the gravure-printed CNT TFT active-matrix backplane described earlier, a large-area compliant tactile sensor array has been successfully demonstrated by integrating the printed TFT backplane with PSR [Fig. 6(a)] [62]. The active-matrix backplane consists of up to 400 TFTs [Fig. 6(b)] with high yield (97%) and excellent uniformity. The system is capable of detecting pressures ranging from 1 to 20 kPa with a linear sensitivity of 800%/kPa. In addition, due to the mechanical compliance of the hybrid dielectrics, the active-matrix backplane is highly flexible with invariant electrical characteristics when bent to a curvature radius of 1.85 cm. As demonstrated in Fig. 6(c), spatial mapping of the pressure profile can be achieved [Fig. 6(d)].

IV. PRINTED PHYSICAL SENSING E-SKIN

A. Printed Strain and Temperature Sensor

Similar to the printed flexible and stretchable transistors discussed earlier, printed flexible sensors are also an important technology for low-cost, macroscale electronics. To address the challenge of replacing conventional vacuum-based semiconductor fabrication processes, a printed sensor made with inks of organic and/or inorganic materials has been reported [13], [20], [63]–[66].

Nanocarbon-based strain and tactile force sensors are widely studied due to their mechanical flexibility and network structure on flexible films [67]. These sensors have mainly three types of the detection mechanism of resistive [68], [69], capacitive [70], [71], and piezoelectric [72] changes. In addition to the mechanical stretchability, by choosing the materials, biodegradable strain and pressure sensors have been reported [73].

For the temperature sensor, the transistor-based sensor and resistive-type sensor are often developed [18], [74]. Another important factor is selectivity used to measure temperature precisely without affecting the strain caused by bending and stretching the films. One of the approaches has been studied by utilizing the stretchable circuits with strain suppression functionality [75]. Although many types of flexible/stretchable sensors have been proposed, specific examples of inorganic nanomaterial-based printed strain and temperature sensors are introduced in this section.

For a printed strain sensor, silver (Ag) NPs and CNTs inks were mixed together and used to monitor the resistance change as a function of applied strain [Fig. 7(a)] [66]. The underlying mechanism of the observed resistance change under tensile strain is due to the change in tunneling current between the AgNPs. The role of the CNT is to electrically bridge the AgNPs under high tensile strain in order to extend the dynamic range of the sensor. The CNT/AgNP ink was screen-printed and cured at 70 °C to form the strain sensor. For the temperature sensor, the CNT ink was mixed with conductive polymer solution of poly(3, 4-ethylenedioxythiophene) polystyrene sulfonate (PEDOT:PSS) and printed [Fig. 7(b)] [76]. The sensing mechanism for temperature relies on electron hopping at the junction between two different materials (CNT and PEDOT:PSS).

Fig. 7(c) shows the fundamental electrical property of the strain sensor on 0.5-mm-thick silicone rubber with 8 mm length. The resistance of the sensor increases when tensile strain is applied, which is resulted from the enlarged distance between the AgNPs than that of the device in a relaxed state. On the other hand, under compressive strain, the distance between the AgNPs becomes

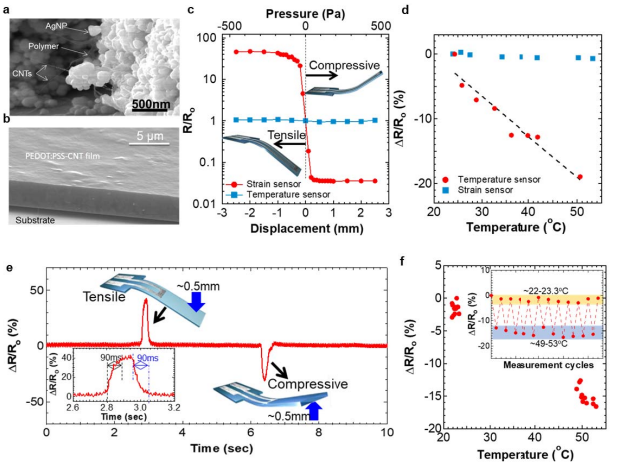

Fig. 7. ***Printed flexible sensors. SEM images of (a) strain sensor and (b) temperature sensor. (c) Resistance change by bending the film for both strain and temperature sensors. (d) Resistance change ratio at different temperatures for each sensor. (e) Real-time resistance change monitoring by applying tensile and compressive strain. Inset: response speed of response and relaxing time. (f) Repeatable resistance change ratio as a function of temperature. Reproduced with permission from [66]. Copyright 2014 American Chemical Society.***

smaller, resulting in decreased resistance. The observed sensor response is in a good agreement with the trend of probability of tunnel current flow between AgNPs depending on the AgNP distance. The resistance change sensitivity of this structure with 4:5 wt% ratio of PEDOT:PSS and CNT inks is ∼59%/Pa. In the case of the temperature sensor, which does not contain AgNPs in the printed film, the resistance change is very small under strain conditions and the corresponding sensitivity is ∼0.02%/Pa [Fig. 7(c)]. On the other hand, the temperature sensor shows a relatively high sensitivity of up to ∼0.63%/°C for the temperature change ranging from 0 °C to 60 °C [Fig. 7(d)] while the strain sensor has a low sensitivity of 0.03%/°C for temperature. Based on the results mentioned above, the high selectivity allows the strain and temperature sensors to be integrated together without interfering each other. Real-time monitoring and repeatability of the strain sensor were analyzed by applying tensile and compressive strain. Fig. 7(e) indicates that the response and release time of strain sensor were less than 90 ms, which is limited by the speed of bending modulated by a hand manually. In addition, the sensor responses were robust and repeatable with stable output for at least 200 cycles of tensile strain. For a printed temperature sensor, the response time depends on the film material but is usually over several seconds due to the low thermal conductivity of the polymer film used. The temperature sensor also exhibited repeatable and stable response with repeated temperature changes confirmed by the experimental results shown in Fig. 7(f). However, it should be noted that both strain and temperature sensors also react to moisture. For practical applications, the passivation layer is required to protect the sensors from moisture.

B. Printed Multifunctional E-Skin

Using the printed strain and temperature sensors, multifunctional printed e-skin was demonstrated, which enables simultaneous detection of tactile force, friction force, and temperature distributions in a single system [18], [20]. For printed multifunctional e-skin, nanocarbon and polymer materials including nanotubes [20], [60], [62], NWs [77], and piezoelectric polymer [18], [78] are dispersed into printed solutions. To realize scalability and multifunctionality especially adding friction force detection, multilayer structures with a suspension sheet, strain sensor sheet, 3-D fingerprintlike structure sheet, and temperature sensor sheet are fabricated, as shown in Fig. 8(a) and (b). Each pixel has four strain sensors, one or two temperature sensors, and a fingerprintlike structure [Fig. 8(c)]. By having the fingerprintlike structure, depending on the force directions of tactile and friction forces, strain distributions are completely different as depicted by the FEM simulation shown in Fig. 8(d) and (e). By recording the strain difference using the strain sensor, tactile force and friction force can be estimated. Furthermore, by monitoring the amplitude of strain, the force amplitude can also be extracted.

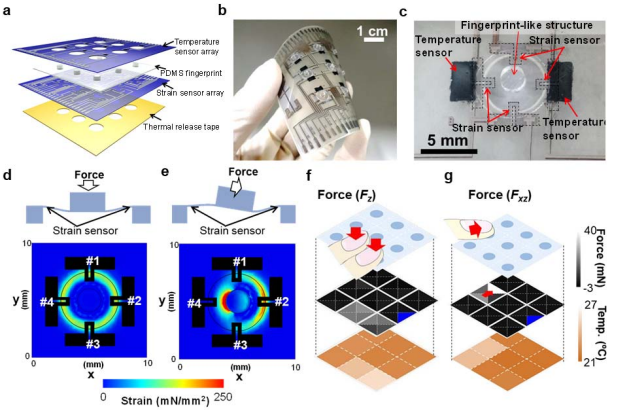

Fig. 8. ***Fully printed e-skin. (a) Schematic and (b) photograph of the printed e-skin with multifunctionality of tactile force, friction force, and temperature monitoring. (c) Zoomed-up image of a pixel integrated with four strain sensors, two temperature sensors, and a fingerprintlike structure. (d) FEM simulations of strain distribution at (d) tactile force and (e) friction force. (f) Tactile and (g) friction force detections using 3 × 3 pixel array with temperature distributions. Reproduced with permission from [20]. Copyright 2014 American Chemical Society.***

Finally, as a proof of concept of the fully printed e-skin with multifunctionality, a 3 × 3 array was demonstrated. To confirm its capability of simultaneously detecting tactile, friction, and temperature distribution, two types of stimuli F_Z and F_{XZ}, representing tactile and friction forces from fingers, respectively, were applied over the fingerprintlike structure. As shown in Fig. 8(f) and (g), when F_Z force was applied, all four strain sensors for each pixel indicated almost the same value. In contrast, when friction force F_{XZ} was applied, asymmetric responses were observed in the four strain sensors in the pixel. These results are in a good agreement with the trend of stress difference at each force direction extracted from the FEM simulations [Fig. 8(d) and (e)]. In addition, temperature distributions were also successfully monitored simultaneously due to the temperature difference between the room environment and fingers.

V. CHEMICAL SENSING E-SKIN

Most of the wearable sensors reported so far focus on monitoring of the vital signs and physical activities and fail to provide the individual's health state at molecular levels. Continuous and real-time monitoring of molecular information is strongly desired for accurately evaluating the user's health conditions. The blood analysis in traditional clinical settings relies on invasive blood draws and cannot provide real-time and continuous information. Human sweat is an important body fluid that can be retrieved conveniently, continuously, and noninvasively. It contains a wealth of chemicals including metabolites, electrolytes, hormones, peptides, and proteins that can reflect the body's physiological state [10], [79], [80]. For example, sweat glucose is currently being intensively

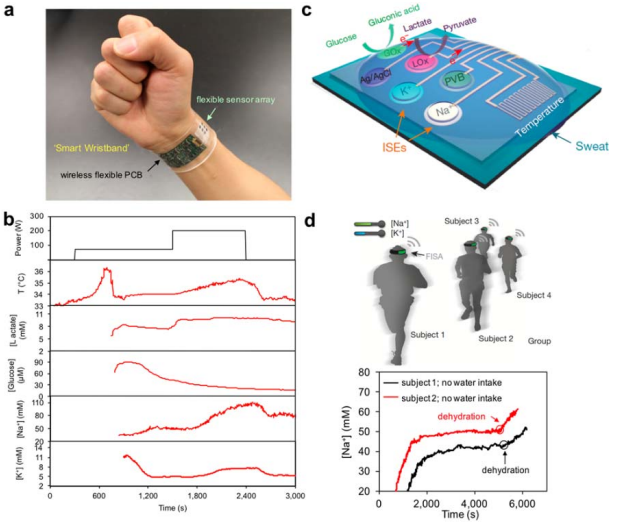

Fig. 9. ***Wearable sensor for multiplexed in situ perspiration analysis. (a) Fully integrated flexible sweat sensor array. (b) Schematic of a sensor array for monitoring of sweat metabolites, electrolytes, as well as skin temperature. (c) Real-time sweat analysis using during a cycling exercise. Reproduced with permission from [7]. (d) Hydration status analysis using the wearable sweat sensor. Copyright 2016 Nature Publishing Group.***

explored for noninvasive glucose monitoring [81]; sweat sodium could be an attractive candidate for monitoring dehydration [82]; sweat chloride is the gold standard for cystic fibrosis diagnosis[83]; sweat test holds great promise in substance abuse monitoring [84], [85]. The transition from the invasive blood analysis to continuous sweat analysis could provide a noninvasive and more attractive means of continuous health monitoring in daily life. In the past three years, tremendous progress has been made toward real-time and continuous monitoring of a broad spectrum of analytes or metabolites (e.g., glucose, lactate, and creatinine), electrolytes (e.g., Na^+, K^+, NH_4^+, Cl^-, pH, and Ca^{2+}), heavy metals (e.g., Cu, Zn, Pb, Hg, and Cd), and small substances (e.g., alcohol and caffeine) [7], [9]–[13], [58]–[61]. The main detection approaches are primarily based on either electrochemical sensing or colorimetric sensing [9], [11]. Bioaffinity sensors can be used for detecting a wide range of proteins, peptides, and hormones but require further development for the deployment in wearable platforms due to the challenges of *in situ* regeneration [53], [54].

A. Chemical Sensor for In Situ Multiplexed Perspiration Analysis

Given the complexity of sweat secretion, the multiplexed detection of target analytes of interest is in urgent need. A fully integrated wearable sensor array was recently developed for *in situ* perspiration analysis [Fig. 9(a)] [7]. Packaged in a wristband or a headband, this mechanically flexible system has conformal contact with the skin and can perform on-site signal conditioning, processing, and wireless transmission. The flexible system simultaneously and selectively measures sweat electrolytes (e.g., Na^+ and K^+) and metabolites (e.g., glucose and lactate), as well as the skin temperature for the real-time signal calibration [Fig. 9(b) and (c)]. The fully integrated wearable sensor platform was successfully used to measure the detailed and dynamic sweat profile of the users in prolonged physical activities and to make a real-time assessment of the physiological state of the individuals. To evaluate the use of this platform for noninvasive monitoring of dehydration, real-time sweat electrolyte (e.g., Na^+) measurements were conducted on the subjects engaged in outdoor running trials [Fig. 9(d)]. Sweat Na^+ levels increased substantially during the exercise when the subjects lost a significant amount of water, indicating that sweat sodium can potentially be used as a key biomarker for dehydration monitoring.

B. Iontophoresis-Based Sweat Sensor

The inherent inaccessibility of a large amount of sweat beyond physical exercise (particularly in sedentary individuals) remains to limit our ability to capitalize on the attractive rich source of physiological information for broad population monitoring. To address this problem, a very promising sweat on-demand extraction method is iontophoresis, which could be used to induce sweat excretion in a small area continuously. The iontophoresis process involves the use of a small electrical current to deliver stimulating agonists (e.g., pilocarpine) to the sweat glands. A wearable sweat extraction and sensing platform has recently been demonstrated by our group, which contains an integrated iontophoresis module able to induce sweat with different profiles at periodic intervals [Fig. 10(a)] [12]. The electrochemical sensing electrodes between the two iontophoresis electrodes allow *in situ* real-time analysis of extracted sweat samples [Fig. 10(b)]. The use of the sweat sensor for the diagnosis of a lung disease—cystic fibrosis—was successfully demonstrated

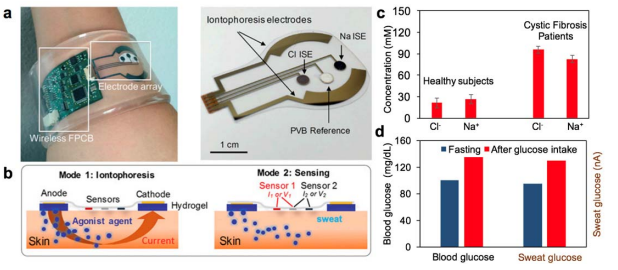

Fig. 10. ***Wearable sweat sensor with an integrated iontophoresis module toward autonomous sweat extraction. (a) Images of the autonomous sweat extraction and sensing platform. (b) Schematic illustrations of the iontophoresis and sensing modes. (c) Screening and diagnosis of cystic fibrosis. (d) Correlation study of sweat and blood glucose levels toward noninvasive glucose monitoring. Reproduced with permission from [12]. Copyright 2017 National Academy of Sciences USA.***

through simultaneous detection of the elevated sweat Na^+ and Cl^- levels [Fig. 10(c)]. The wearable device was also utilized to investigate the correlation between sweat and blood analyte levels (i.e., glucose). It was shown that oral glucose intake in fasting subjects resulted in a significant increase in glucose level in both blood and sweat [Fig. 10(d)].

C. Sweat Sensor for Drug Analysis

Wearable sweat sensors have great promise in real-time and continuous drug monitoring for doping control and precision medicine. Drug analysis is commonly implemented for drug abuse testing, doping control, and chemotherapy. Conventional drug monitoring relies on the invasive blood test and time-consuming instrumental analysis. Sweat is an attractive alternative biofluid that could provide real-time information of the drug dosage and drug metabolism. A wearable sweatband was developed for noninvasive and dynamic monitoring of drug levels [Fig. 11(a)] [88]. Caffeine was selected as a model methylxanthine drug to demonstrate the sensor's capabilities. The detection of caffeine is achieved by measuring the oxidation of caffeine through differential pulse voltammetry (DPV). Sweat caffeine levels increased with the increase in drug dosage, and the confirmable caffeine physiological trends over time after the intake were observed [Fig. 11(b)]. Such wearable sweat sensor was capable of monitoring the dynamic drug levels over time [Fig. 11(c)].

D. *In Situ* Sweat Sampling and Sweat Rate Sensing

Proper sweat sampling is critical to improve the temporal resolution of the sweat analysis and to minimize the errors caused by sweat evaporation and skin contamination. In addition, sweat compositions and sweat rate are found to be inextricably linked. In order to achieve enhanced sweat sampling and dynamic sweat rate monitoring, a flexible and wearable microfluidic sweat sensing patch has been developed recently [89]. As sweat travels along the microchannel, the electrical impedance measured between two parallel electrodes in the microchannel drops as the sweat volume increases due to the increase in the capacitance and the decrease in the effective resistance. Sweat rate was calculated as the sweat volume changes in the microchannel divided by the time interval. System integration of chemical sensing and electroimpedance measurement in a single device greatly facilitates the *in situ* sweat analysis. Such sweat patch could provide a comprehensive sweat secretion information for a number of fundamental and clinical investigations.

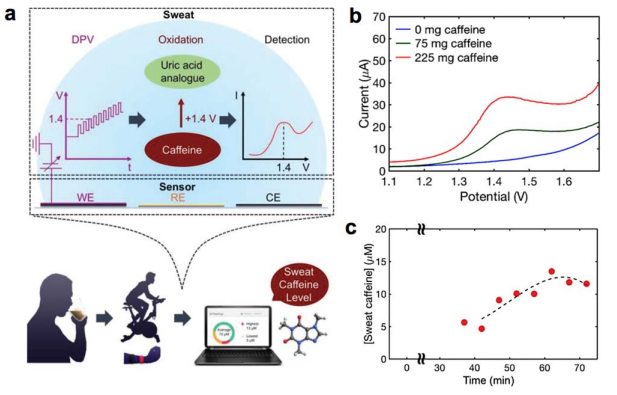

Fig. 11. ***Methylxanthine drug monitoring with wearable sweat sensors. (a) Electrochemical detection of caffeine through DPV. Oxidation of caffeine leads to an observable oxidation peak around 1.4 V. (b) Sensor response in human sweat samples for all caffeine intake conditions. (c) Summary plot of the sweat caffeine levels over time during the exercise after caffeine intake. Reproduced with permission from [87]. Copyright 2018 John Wiley and Sons.***

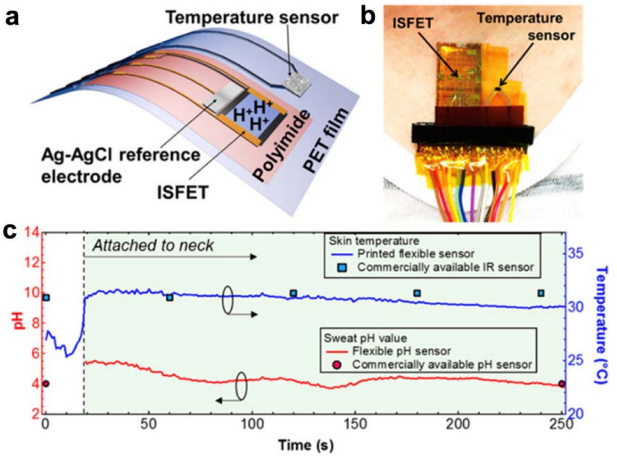

Fig. 12. ***Flexible and multifunctional healthcare device with an ISFET chemical sensor for simultaneous sweat pH and skin temperature monitoring. (a) Schematic of a wearable device integrating flexible pH and temperature sensors. (b) Photograph showing the attachment of the flexible pH and temperature sensors to the test subject's neck. (c) Real-time pH and skin temperature information acquired by the wearable device. Reproduced with permission from [90]. Copyright 2017 American Chemical Society.***

E. Fusion of Sweat Chemical Sensor and Physical Sensor

In practical biomedical applications, acquiring both molecular information of the human body, alongside physical characteristics such as vital signs, is extremely critical for accurately identifying health conditions [7]. Moreover, the measured information from one sensor could potentially be used to calibrate the readings of other sensors. For example, a flexible ion-sensitive field-effect transistor (ISFET)-based pH sensor was developed and integrated with a flexible skin temperature sensor to monitor both skin temperatures to compensate the temperature effect of the ISFET for accurate measurement [Fig. 12] [90].

For the ISFET, an Al_2O_3 layer was used for the pH sensing membrane, while an InGaZnO thin film was used as the n-type FET material. Moving toward the realization of personalized medicine, the integration of more functionality and sensing modality into the flexible e-skin system, such as accelerometers, other vital sign and chemical sensors, and signal processing circuits, is needed.

VI. CONCLUSION

In this paper, we have explained and highlighted the recent progress on flexible and stretchable physical and chemical sensors for e-skin applications, with the emphasis on the design and selection of materials and structures and the integration of various types of sensor and circuits. This paper also introduced a few key potential applications of the e-skin in robotics and healthcare. With its scalability, low cost, multifunctionality, and the desirable form factor of a flexible or stretchable sheet, such physical and chemical sensing e-skin can be applied to many different applications, especially for "IoT" to collect information from any surfaces or objects.

For practical application of this e-skin concept, many issues such as integrating more sensing modalities, improving device reliability, and reducing motion artifacts, and feedback and interaction between human and e-skin through artificial intelligence and deep learning still need to be addressed. In particular, e-skin developments are mainly conducted by academia. However, to achieve the practical platform for e-skin applied to robotics, healthcare, and industry, long-time stability and reliability including the uniformity of the fabrication should be addressed while more functionalities, power generation, and circuit systems are in parallel developed with the consideration of their integrations on flexible and stretchable films. To open the technologies to the market, deep collaboration works between academia and industries are required to support each weakness of the developments. Furthermore, key applications should be proposed to use the flexible electronic systems by building new concepts or replacing conventional electronic systems [91]. Without showing this concept, it is hard to move forward to developing the flexible electronic systems. Although a lot of developments are required, we believe that the described technologies and concepts may lead us toward realizing the next class of low-cost, multifunctional, macroscale, and stretchable e-skin. ■

REFERENCES

[1] T. Someya *et al.*, "Conformable, flexible, large-area networks of pressure and thermal sensors with organic transistor active matrixes," *Proc. Nat. Acad. Sci. USA*, vol. 102, no. 35, pp. 12321–12325, 2005.

[2] K. Takei *et al.*, "Nanowire active-matrix circuitry for low-voltage macroscale artificial skin," *Nature Mater.*, vol. 9, no. 10, pp. 821–826, 2010.

[3] D.-H. Kim *et al.*, "Epidermal electronics," *Science*, vol. 333, no. 6044, pp. 838–843, 2011.

[4] M. Kaltenbrunner *et al.*, "An ultra-lightweight design for imperceptible plastic electronics," *Nature*, vol. 499, no. 7459, pp. 458–463, Jul. 2013.

[5] A. Chortos, J. Liu, and Z. Bao, "Pursuing prosthetic electronic skin," *Nature Mater.*, vol. 15, pp. 937–950, Jul. 2016.

[6] T. Sekitani and T. Someya, "Stretchable, large-area organic electronics," *Adv. Mater.*, vol. 22, no. 20, pp. 2228–2246, 2010.

[7] W. Gao *et al.*, "Fully integrated wearable sensor arrays for multiplexed *in situ* perspiration analysis," *Nature*, vol. 529, pp. 509–514, Jan. 2016.

[8] Y. Yamamoto *et al.*, "Printed multifunctional flexible device with an integrated motion sensor for health care monitoring," *Sci. Adv.*, vol. 2, no. 11, 2016, Art. no. e1601473.

[9] Y. Yang and W. Gao, "Wearable and flexible electronics for continuous molecular monitoring," *Chem. Soc. Rev.*, vol. 48, pp. 1465–1491, 2019.

[10] M. Bariya, H. Y. Y. Nyein, and A. Javey, "Wearable sweat sensors," *Nat. Electron.*, vol. 1, no. 3, pp. 160–171, 2018.

[11] J. Choi, R. Ghaffari, L. B. Baker, and J. A. Rogers, "Skin-interfaced systems for sweat collection and analytics," *Sci. Adv.*, vol. 4, no. 2, 2018, Art. no. eaar3921.

[12] S. Emaminejad *et al.*, "Autonomous sweat extraction and analysis applied to cystic fibrosis and glucose monitoring using a fully integrated wearable platform," *Proc. Nat. Acad. Sci. USA*, vol. 114, no. 18, pp. 4625–4630, 2017.

[13] K. Takei, Z. Yu, M. Zheng, H. Ota, T. Takahashi, and A. Javey, "Highly sensitive electronic whiskers based on patterned carbon nanotube and silver nanoparticle composite films," *Nat. Acad. Sci. USA*, vol. 111, no. 5, pp. 1703–1707, 2014.

[14] C. Wang *et al.*, "User-interactive electronic skin for instantaneous pressure visualization," *Nature Mater.*, vol. 12, pp. 899–904, Jul. 2013.

[15] D. H. Kim *et al.*, "Materials for multifunctional balloon catheters with capabilities in cardiac electrophysiological mapping and ablation therapy," *Nature Mater.*, vol. 10, no. 4, pp. 316–323, Apr. 2011.

[16] K. Kanao, S. Nakata, T. Arie, S. Akita, and K. Takei, "Human-interactive multi-functional electronic wallpaper integrated with sensors and memory," *Mater. Horizons*, vol. 4, no. 6, pp. 1079–1084, 2017.

[17] J.-W. Jeong *et al.*, "Materials and optimized designs for human-machine interfaces via epidermal electronics," *Adv. Mater.*, vol. 25, no. 47, pp. 6839–6846, Dec. 2013.

[18] J. Park, M. Kim, Y. Lee, H. S. Lee, and H. Ko, "Fingertip skin–inspired microstructured ferroelectric skins discriminate static/dynamic pressure and temperature stimuli," *Sci. Adv.*, vol. 1, no. 9, 2015, Art. no. e1500661.

[19] T. Yokota *et al.*, "Ultraflexible, large-area, physiological temperature sensors for multipoint measurements," *Proc. Nat. Acad. Sci. USA*, vol. 112, no. 47, pp. 14533–14538, 2015.

[20] S. Harada, K. Kanao, Y. Yamamoto, T. Arie, S. Akita, and K. Takei, "Fully printed flexible fingerprint-like three-axis tactile and slip force and temperature sensors for artificial skin," *ACS Nano*, vol. 8, no. 12, pp. 12851–12857, 2014.

[21] C. M. Boutry *et al.*, "A hierarchically patterned, bioinspired e-skin able to detect the direction of applied pressure for robotics," *Sci. Robot.*, vol. 3, no. 24, 2018, Art. no. eaau6914.

[22] R. D. Giacomo, L. Bonanomi, V. Costanza, B. Baresca, and C. Daraio, "Biomimetic temperature sensing layer for artificial skins," *Sci. Robot.*, vol. 2, Sep. 2017, Art. no. eaai9251.

[23] Y.-C. Lai *et al.*, "Actively perceiving and responsive soft robots enabled by self-powered, highly extensible, and highly sensitive triboelectric proximity- and pressure-sensing skins," *Adv. Mater.*, vol. 30, no. 28, 2018, Art. no. 1801114.

[24] G. Schwartz *et al.*, "Flexible polymer transistors with high pressure sensitivity for application in electronic skin and health monitoring," *Nature Commun.*, vol. 4, p. 1859, May 2013.

[25] T. Takahashi, K. Takei, A. G. Gillies, R. S. Fearing, and A. Javey, "Carbon nanotube active-matrix backplanes for conformal electronics and sensors," *Nano Lett.*, vol. 11, no. 12, pp. 5408–5413, 2011.

[26] Y. J. Park *et al.*, "All MoS_2 based large area, skin-attachable active-matrix tactile sensor," *ACS Nano*, vol. 13, no. 3, pp. 3023–3030, 2019.

[27] J. A. Rogers, M. G. Lagally, and R. G. Nuzzo, "Synthesis, assembly and applications of semiconductor nanomembranes," *Nature*, vol. 477, no. 7362, pp. 45–53, 2011.

[28] H. H. Chou *et al.*, "A chameleon-inspired stretchable electronic skin with interactive colour changing controlled by tactile sensing," *Nature Commun.*, vol. 6, Aug. 2015, Art. no. 8011.

[29] A. C. Arias, J. D. Mackenzie, I. McCulloch, J. Rivnay, and A. Salleo, "Materials and applications for large area electronics: Solution-based approaches," *Chem. Rev.*, vol. 110, no. 1, pp. 3–24, 2010.

[30] M. Singh, H. M. Haverinen, P. Dhagat, and G. E. Jabbour, "Inkjet printing-process and its applications," *Adv. Mater.*, vol. 22, no. 6, pp. 673–685, 2010.

[31] S. R. Forrest, "The path to ubiquitous and low-cost organic electronic appliances on plastic," *Nature*, vol. 428, pp. 911–918, Apr. 2004.

[32] K. Y. Chun, Y. Oh, J. Rho, J. H. Ahn, Y. J. Kim, and H. R. Choi, "Highly conductive, printable and stretchable composite films of carbon nanotubes and silver," *Nature Nanotechnol.*, vol. 5, pp. 853–857, Dec. 2010.

[33] P. Lee *et al.*, "Highly stretchable and highly conductive metal electrode by very long metal nanowire percolation network," *Adv. Mater.*, vol. 24, no. 25, pp. 3326–3332, 2012.

[34] F. Xu and Y. Zhu, "Highly conductive and stretchable silver nanowire conductors," *Adv. Mater.*, vol. 24, no. 37, pp. 5117–5122, 2012.

[35] S. Yao and Y. Zhu, "Nanomaterial-enabled stretchable conductors: Strategies, materials and devices," *Adv. Mater.*, vol. 27, no. 9, pp. 1480–1511, 2015.

[36] S. Bae *et al.*, "Roll-to-roll production of 30-inch graphene films for transparent electrodes," *Nature Nanotechnol.*, vol. 5, no. 8, pp. 574–578, Jun. 2010.

[37] D. J. Lipomi, J. A. Lee, M. Vosgueritchian, B. C.-K. Tee, J. A. Bolander, and Z. Bao, "Electronic properties of transparent conductive films of PEDOT:PSS on stretchable substrates," *Chem. Mater.*, vol. 24, no. 2, pp. 373–382, 2012.

[38] Y. Wang *et al.*, "A highly stretchable, transparent, and conductive polymer," *Sci. Adv.*, vol. 3, Mar. 2017, Art. no. e1602076.

[39] T. Sekitani, Y. Noguchi, K. Hata, T. Fukushima, T. Aida, and T. Someya, "A rubberlike stretchable active matrix using elastic conductors," *Science*, vol. 321, pp. 1468–1472, Sep. 2008.

[40] Y. Kim *et al.*, "Stretchable nanoparticle conductors with self-organized conductive pathways," *Nature*, vol. 500, pp. 59–63, Aug. 2013.

[41] M. Ha *et al.*, "Printed, sub-3V digital circuits on plastic from aqueous carbon nanotube inks," *ACS Nano*, vol. 4, no. 8, pp. 4388–4395, 2010.

[42] R. P. Ortiz, A. Facchetti, and T. J. Marks, "High-k organic, inorganic, and hybrid dielectrics for low-voltage organic field-effect transistors," *Chem. Rev.*, vol. 110, no. 1, pp. 205–239, Jan. 2010.

[43] H. Klauk, "Organic thin-film transistors," *Chem. Soc. Rev.*, vol. 39, no. 7, pp. 2643–2666, Apr. 2010.

[44] H. Sirringhaus, T. Kawase, R. H. Friend, T. Shimoda, M. Inbasekaran, and W. Wu, "High-resolution inkjet printing of all-polymer transistor circuits," *Science*, vol. 290, pp. 2123–2127, Dec. 2000.

[45] Z. Fan *et al.*, "Toward the development of printable nanowire electronics and sensors," *Adv. Mater.*, vol. 21, no. 37, pp. 3730–3743, 2009.

[46] K. Chen *et al.*, "Printed carbon nanotube electronics and sensor systems," *Adv. Mater.*, vol. 28, pp. 4397–4414, Jun. 2016.

[47] A. G. Kelly *et al.*, "All-printed thin-film transistors from networks of liquid-exfoliated nanosheets," *Science*, vol. 356, pp. 69–73, Apr. 2017.

[48] P. Vuttipittayamongkol, F. Wu, H. Chen, X. Cao, B. Liu, and C. Zhou, "Threshold voltage tuning and printed complementary transistors and inverters based on thin films of carbon nanotubes and indium zinc oxide," *Nano Res.*, vol. 8, no. 4, pp. 1159–1168, Oct. 2014.

[49] H. Okimoto *et al.*, "Tunable carbon nanotube thin-film transistors produced exclusively via inkjet printing," *Adv. Mater.*, vol. 22, no. 36, pp. 3981–3986, 2010.

[50] P. Chen *et al.*, "Fully printed separated carbon nanotube thin film transistor circuits and its application in organic light emitting diode control," *Nano Lett.*, vol. 11, pp. 5301–5308, Nov. 2011.

[51] M. Jung, J. Kim, J. Noh, N. Lim, C. Lim, and G. Y. Lee, "All-printed and roll-to-roll-printable 13.56-MHz-operated 1-bit RF tag on plastic foils," *IEEE Trans. Electron Devices*, vol. 57, no. 3, pp. 570–580, Mar. 2010.

[52] J. Noh, S. Kim, K. Jung, J. Kim, S. Cho, and G. Cho, "Fully gravure printed half adder on plastic foils," *IEEE Electron Device Lett.*, vol. 32, no. 11, pp. 1555–1557, Nov. 2011.

[53] J. Noh *et al.*, "Fully gravure-printed D flip-flop on plastic foils using single-walled carbon-nanotube-based TFTs," *IEEE Electron Device Lett.*, vol. 32, no. 5, pp. 638–640, May 2011.

[54] P. H. Lau *et al.*, "Fully printed, high performance carbon nanotube thin-film transistors on flexible substrates," *Nano Lett*, vol. 13, pp. 3864–3869, Aug. 2013.

[55] M. Ha *et al.*, "Aerosol jet printed, low voltage, electrolyte gated carbon nanotube ring oscillators with sub-5 μs stage delays," *Nano Lett.*, vol. 13, pp. 954–960, Feb. 2013.

[56] X. D. Cao *et al.*, "Screen printing as a scalable and low-cost approach for rigid and flexible thin-film transistors using separated carbon nanotubes," *ACS Nano*, vol. 8, pp. 12769–12776, Dec. 2014.

[57] M. L. Hammock, A. Chortos, B. C.-K. Tee, J. B.-H. Tok, and Z. Bao, "25th anniversary article: The evolution of electronic skin (E-Skin): A brief history, design considerations, and recent progress," *Adv. Mater.*, vol. 25, no. 42, pp. 5997–6038, Nov. 2013.

[58] J. Liang, L. Li, X. Niu, Z. Yu, and Q. Pei, "Elastomeric polymer light-emitting devices and displays," *Nature Photon.*, vol. 7, no. 10, pp. 817–824, Sep. 2013.

[59] N. Matsuhisa *et al.*, "Printable elastic conductors with a high conductivity for electronic textile applications," *Nature Commun.*, vol. 6, no. 1, p. 7461, Dec. 2015.

[60] T. Yamada *et al.*, "A stretchable carbon nanotube strain sensor for human-motion detection," *Nature Nanotechnol.*, vol. 6, pp. 296–301, Mar. 2011.

[61] L. Cai, S. Zhang, J. Miao, Z. Yu, and C. Wang, "Fully printed stretchable thin-film transistors and integrated logic circuits," *ACS Nano*, vol. 10, no. 12, pp. 11459–11468, 2016.

[62] C. Yeom, K. Chen, D. Kiriya, Z. Yu, G. Cho, and A. Javey, "Large-area compliant tactile sensors using printed carbon nanotube active-matrix backplanes," *Adv. Mater.*, vol. 27, no. 9, pp. 1561–1566, 2015.

[63] D. Karnaushenko, D. Makarov, M. Stöber, D. D. Karnaushenko, S. Baunack, and O. G. Schmidt, "High-performance magnetic sensorics for printable and flexible electronics," *Adv. Mater.*, vol. 27, no. 5, pp. 880–885, 2014.

[64] W. Wu, "Inorganic nanomaterials for printed electronics: A review," *Nanoscale*, vol. 9, no. 22, pp. 7342–7372, 2017.

[65] X. Liu, L. Gu, Q. Zhang, J. Wu, Y. Long, and Z. Fan, "All-printable band-edge modulated ZnO nanowire photodetectors with ultra-high detectivity," *Nature Commun.*, vol. 5, p. 4007, Sep. 2014.

[66] S. Harada, W. Honda, T. Arie, S. Akita, and K. Takei, "Fully printed, highly sensitive multifunctional artificial electronic whisker arrays integrated with strain and temperature sensors," *ACS Nano*, vol. 8, no. 4, pp. 3921–3927, 2014.

[67] C. M. Boutry, M. Negre, M. Jorda, O. Vardoulis, A. Chortos, and O. Khatib, "A hierarchically patterned, bioinspired e-skin able to detect the direction of applied pressure for robotics," *Sci. Robot.*, vol. 3, no. 24, 2018, Art. no. eaau6914.

[68] M. Liu *et al.*, "Large-area all-textile pressure sensors for monitoring human motion and physiological signals," *Adv. Mater.*, vol. 29, no. 41, 2017, Art. no. 1703700.

[69] H. Song *et al.*, "Superfast and high-sensitivity printable strain sensors with bioinspired micron-scale cracks," *Nanoscale*, vol. 9, no. 3, pp. 1166–1173, 2016.

[70] S. Pyo, J. Choi, and J. Kim, "Flexible, transparent, sensitive, and crosstalk-free capacitive tactile sensor array based on graphene electrodes and air dielectric," *Adv. Electron. Mater.*, vol. 4, no. 1, 2017, Art. no. 1700427.

[71] M. R. Kulkarni, R. A. John, M. Rajput, N. Tiwari, N. Yantara, and A. C. Nguyen, "Transparent flexible multifunctional nanostructured architectures for non-optical readout, proximity, and pressure sensing," *ACS Appl. Mater. Interfaces*, vol. 9, no. 17, pp. 15015–15021, 2017.

[72] X. Wang, H. Zhang, L. Dong, X. Han, W. Du, and J. Zhai, "Self-powered high-resolution and pressure-sensitive triboelectric sensor matrix for real-time tactile mapping," *Adv. Mater.*, vol. 28, no. 15, pp. 2896–2903, 2016.

[73] C. M. Boutry *et al.*, "A stretchable and biodegradable strain and pressure sensor for orthopaedic application," *Nature Electron.*, vol. 1, no. 5, pp. 314–321, 2018.

[74] X. Ren *et al.*, "A low-operating-power and flexible active-matrix organic-transistor temperature-sensor array," *Adv. Mater.*, vol. 28, no. 24, pp. 4832–4838, Apr. 2016.

[75] C. Zhu *et al.*, "Stretchable temperature-sensing circuits with strain suppression based on carbon nanotube transistors," *Nature Electron.*, vol. 1, no. 3, pp. 183–190, 2018.

[76] W. Honda, S. Harada, T. Arie, S. Akita, and K. Takei, "Wearable, human-interactive, health-monitoring, wireless devices fabricated by macroscale printing techniques," *Adv. Funct. Mater.*, vol. 24, pp. 3299–3304, Jun. 2014.

[77] K. K. Kim *et al.*, "Highly sensitive and stretchable multidimensional strain sensor with prestrained anisotropic metal nanowire percolation networks," *Nano Lett.*, vol. 15, no. 8, pp. 5240–5247, 2015.

[78] Y. Huang, Y. Ding, J. Bian, Y. Su, J. Zhou, and Y. Duan, "Hyper-stretchable self-powered sensors based on electrohydrodynamically printed, self-similar piezoelectric nano/microfibers," *Nano Energy*, vol. 40, pp. 432–439, Oct. 2017.

[79] J. Heikenfeld, "Non-invasive analyte access and sensing through eccrine sweat: Challenges and outlook circa 2016," *Electroanalysis*, vol. 28, no. 6, pp. 1242–1249, 2016.

[80] A. J. Bandodkar, I. Jeerapan, and J. Wang, "Wearable chemical sensors: Present challenges and future prospects," *ACS Sens.*, vol. 1, no. 5, pp. 464–482, 2016.

[81] H. Lee *et al.*, "A graphene-based electrochemical device with thermoresponsive microneedles for diabetes monitoring and therapy," *Nature Nanotechnol.*, vol. 11, no. 6, pp. 566–572, Jun. 2016.

[82] R. M. Morgan, M. J. Patterson, and M. A. Nimmo, "Acute effects of dehydration on sweat composition in men during prolonged exercise in the heat," *Acta Physiol. Scandinavica*, vol. 182, no. 1, pp. 37–43, 2004.

[83] A. A. Green, P. Dodds, and C. Pennock, "A study of sweat sodium and chloride; criteria for the diagnosis of cystic fibrosis," *Ann. Clin. Biochem.*, vol. 22, no. 2, pp. 171–176, 1985.

[84] N. De Giovanni and N. Fucci, "The current status of sweat testing for drugs of abuse: A review," *Current Med. Chem.*, vol. 20, no. 4, pp. 545–561, 2013.

[85] J. Kim *et al.*, "Noninvasive alcohol monitoring using a wearable tattoo-based iontophoretic-biosensing system," *ACS Sensors*, vol. 1, no. 8, pp. 1011–1019, 2016.

[86] W. Gao *et al.*, "Wearable microsensor array for multiplexed heavy metal monitoring of body fluids," *ACS Sensors*, vol. 1, no. 7, pp. 866–874, 2016.

[87] H. Y. Nyein, W. Gao, Z. Shahpar, S. Emaminejad, S. Challa, and K. Chen, "A wearable electrochemical platform for noninvasive simultaneous monitoring of Ca^{2+} and pH," *ACS Nano*, vol. 10, no. 7, pp. 7216–7224, 2016.

[88] L.-C. Tai *et al.*, "Methylxanthine drug monitoring with wearable sweat sensors," *Adv. Mater.*, vol. 30, no. 23, 2018, Art. no. 1707442.

[89] H. Y. Y. Nyein *et al.*, "A wearable microfluidic sensing patch for dynamic sweat secretion analysis," *ACS Sensors*, vol. 3, no. 5, pp. 944–952, 2018.

[90] S. Nakata, T. Arie, S. Akita, and K. Takei, "Wearable, flexible, and multifunctional healthcare device with an ISFET chemical sensor for simultaneous sweat pH and skin temperature monitoring," *ACS Sensors*, vol. 2, no. 3, pp. 443–448, 2017.

[91] R. Dahiya, "E-Skin: From humanoids to humans," *Proc. IEEE*, vol. 107, no. 2, pp. 247–252, Feb. 2019.

ABOUT THE AUTHORS

Kuniharu Takei (Member, IEEE) is currently a Professor with the Department of Physics and Electronics, Osaka Prefecture University, Osaka, Japan. His current research interests include printed and flexible electronics, human-interactive devices, soft robotics, and micro/nanomaterial devices.

Prof. Takei was a recipient of some awards, including the Technology Review TR35 (35 innovators under 35) in 2013, NISTEP Researcher 2015 by the Minister of Education, Culture, Sports, Science and Technology (MEXT), and the Young Scientists' Prize of the Commendation for Science and Technology by MEXT in 2018.

Wei Gao received the Ph.D. degree in chemical engineering with the University of California at San Diego, San Diego, CA, USA, in 2014, as a Jacobs Fellow and HHMI International Student Research Fellow.

From 2014 to 2017, he was a Postdoctoral Fellow with the Department of Electrical Engineering and Computer Sciences, University of California at Berkeley, Berkeley, CA, USA. He is currently an Assistant Professor of medical engineering with the Division of Engineering and Applied Science, California Institute of Technology, Pasadena, CA, USA. His current research interests include wearable devices, biosensors, flexible electronics, micro/nanorobotics, and nanomedicine.

Dr. Gao was a recipient of the 2018 Sensors Young Investigator Award, the 2016 MIT Technology Review 35 Innovators Under 35 (TR35), and the 2015 ACS Young Investigator Award (Division of Inorganic Chemistry).

Chuan Wang received the B.S. degree in microelectronics from Peking University, Beijing, China, in 2005, and the Ph.D. degree in electrical engineering from the University of Southern California, Los Angeles, CA, USA, in 2011.

From 2011 to 2013, he was a Postdoctoral Scholar with the Department of Electrical Engineering and Computer Sciences, University of California at Berkeley, Berkeley, CA, USA. From 2013 to 2018, he was an Assistant Professor of electrical and computer engineering with Michigan State University, East Lansing, MI, USA. He is currently an Assistant Professor of electrical and systems engineering with Washington University in St. Louis, St. Louis, MO, USA. His current research interests include stretchable electronics and printed electronics for displaying, sensing, and energy harvesting applications, and 2-D semiconductor nanoelectronics and optoelectronics.

Ali Javey is currently a Professor of electrical engineering and computer sciences with the University of California at Berkeley, Berkeley, CA, USA. He is also a Faculty Scientist with the Lawrence Berkeley National Laboratory, University of California at Berkeley, where he serves as the Program Leader of electronic materials (E-Mat). He is the Co-Director of the Berkeley Sensor and Actuator Center (BSAC), University of California at Berkeley, and Bay Area PV Consortium (BAPVC), USA.

Prof. Javey was a recipient of the MRS Outstanding Young Investigator Award in 2015, the Nano Letters Young Investigator Lectureship in 2014, the APEC Science Prize for Innovation, Research, and Education in 2011, the Netexplorateur of the Year Award in 2011, the IEEE Nanotechnology Early Career Award in 2010, the National Academy of Sciences Award for Initiatives in Research in 2009, the Technology Review TR35 in 2009, the NSF Early CAREER Award in 2008, and the U.S. Frontiers of Engineering by National Academy of Engineering in 2008. He is an Associate Editor of *ACS Nano*.